Peer-reviewed version available at *Minerals* **2019**, *9*, 724; doi:10.3390/min9120724

Determination of Size Distribution of Precipitation Aggregates Using Non-Invasive Microscopy and Semiautomated Image Processing and Analysis

Michelle Quilaqueo[1], Minghai Gim-Krumm[1,2], René Ruby-Figueroa[3], Elizabeth Troncoso[2,3*], Humberto Estay [1*]

[1]Advanced Mining Technology Center (AMTC), University of Chile, Av. Tupper 2007 (AMTC Building), Santiago, Chile.

[2]Department ofChemistry, Universidad Tecnológica Metropolitana, Las Palmeras 3360, Ñuñoa, Santiago, Chile.

[3]Programa Institucional de Fomento a la Investigación, Desarrollo e Innovación, Universidad Tecnológica Metropolitana, Ignacio Valdivieso 2409, San Joaquín, Santiago, Chile.

[*]Corresponding authors:

Dr. Humberto Estay, Advanced Mining Technology Center (AMTC), University of Chile, Tupper 2007 (AMTC Building), Santiago, Chile. E-mail: humberto.estay@amtc.cl

Dr. Elizabeth Troncoso, DepartmentofChemistry, Universidad Tecnológica Metropolitana, Las Palmeras 3360, Ñuñoa, Santiago, Chile.E-mail: elizabeth.troncoso@utem.cl

Abstract

Precipitation processes are technologies commonly used in hydrometallurgical plants to recover metals or to treat wastewaters. Moreover, solid-liquid separation technologies, such as thickening or filtering, are relevant unit operations, included in the precipitation technologies. These methods are strongly dependent on the characteristics of the solid precipitates formed during the specific precipitation reaction. One of these characteristics is the particle size distribution (PSD) of the solid precipitates which are fed into a solid-liquid separation process. Therefore, PSD determination is a typical practice for the characterization of the slurries generated in a precipitation plant. Furthermore, the precipitates generated in these processes have a colloidal or aggregation behavior, depending on the operational conditions. Nevertheless, the conventional methods used to estimate PSD (e.g., laser diffraction and/or ciclosizer) have not been designed to measure particles that tend to aggregate or disaggregate, since they include external forces (e.g., centrifugal, agitation, pumping and sonication). These forces affect the true size of the aggregates formed in a unit operation, thereby losing representativity in terms of aggregates particle size. This study presents an alternative method of measuring the size distribution of particles with aggregation behavior, particularly, by using non-invasive microscopy and image processing and analysis. The samples used have been obtained from an experimental precipitation process by applying sulfidization to treat the cyanide-copper complexes contained in a cyanidation solution. This method has been validated with statistical tools and compared with a conventional analysis based on laser diffraction. Our results show significant differences between the methods analyzed, demonstrating that image processing and analysis by microscopy is an excellent and non-invasive alternative to obtaining size distribution of aggregates in precipitation processes.

Keywords: SART process; precipitation aggregates; image analysis; microscopy; particle size distribution

1. Introduction

1.1 Background

The precipitation process is one of the technological options available for treating solutions in hydrometallurgical plants, with the purpose of recovering or removing metals, among others compounds **[1]**. Typical applications are found in gold cementation, using zinc powder **[2]**; copper cementation, using scrap iron **[1]**; acid mine drainage (AMD) treatment, using milk of lime **[3]**; copper sulfide precipitation from acid mine drainage, using hydrogen sulfide **[4];** and copper sulfide precipitation from cyanide solutions in gold mining **[5]**. These processes must accommodate a subsequent solid-liquid separation stage (i.e., thickeners and/or filters) to remove the solids generated from the solution. The characteristics of these precipitates (colloidal behavior and fine particles) determine the thickeners, large filter size, and rigorous operational control required in order to prevent a high content of suspended solids in the recovered solutions **[6-9]**. Particularly, the copper sulfide precipitation process from acid mine drainage and cyanide solutions is very attractive, owing to its capacity to recover valuable by-products from wastewaters (in the case of AMD) and gold mining (in the case of cyanide solutions). An appropriate characterization of the precipitate size is crucial for the selection and design of an adequate separation process. In this context, there are some studies that characterize the precipitates formed in sulfidization processes for treating AMD **[6,7]** and cyanide solutions **[9]**. These studies determined the aggregate characteristics from metal sulfide precipitates and the dependence of pH and sulfide dosage (chemical solution characteristics) on aggregate size. Thus, settling rate results determined

by operational conditions related to pH and sulfide dosage. These results indicate the relevance of the aggregate size to operational conditions when operating and designing solid-liquid separation equipment. For this reason, the experimental technique used to quantify particle size and particle size distribution could play a critical role in the interpretation of data, which may underestimate or overestimate set-points for chosen operational conditions when operating solid-liquid separation equipment. Unfortunately, the methodologies currently used to measure particle size and particle size distribution (PSD) of fine particles (0.1 - 100 µm), such as Malvern Mastersizer (MMS) or cyclosizer (CS), have been designed to quantify PSD, but not to measure aggregate size distribution (ASD). This quantification is crucial when defining optimal operational conditions for thickening process. The two methods mentioned above (MMS and CS) involve external forces (e.g., agitation, pumping and centrifugal in the case of CS) which can affect the physical integrity of the aggregates, and consequently alter their size distribution. A previous study shows the impact of CS on the mineral's surface, owing to the external forces applied to separate particles of different sizes **[10]**. However, the Focused Beam Reflectance Measurement (FBRM) allows the aggregate size distribution to be determined, although this technique is still very expensive for experimental and research purposes. Hence, it is necessary to quantify the ASD using non-invasive and less expensive techniques than FBRM. In this context, this study proposes a new non-invasive method to quantify size distribution of aggregates using microscopy and semiautomated image processing and analysis.

1.2 Particle size distribution using microscopy and image processing and analysis

The measurement of particle or aggregate size distribution is not a simple task, because it depends on a series of factors which affect the measurement. As mentioned above, these

97 factors include the heterogeneity of the sample itself as well as the strategy employed to make
98 the results representative of the sample's characteristics. In this regard, microscopy is a
99 technique that has not only been used as a powerful tool when morphological information is
100 required to understand the behavior of a material (such as civil engineering materials) **[11,12]**
101 or in the electronics industry **[13],** but also to quantify the particle size distribution
102 successfully in various fields, such as food, pharmaceuticals, and mineral processing. For
103 example, microscopy has been employed to quantify microstructures and correlate them with
104 rheological properties in apple tissue **[14]**. Also, microscopy has been applied to determine
105 the bubble size distribution in aerated whey protein gels **[15]**. Moreover, successful
106 applications have also been reported regarding the measurement of soil grain-size
107 distribution, in which no significant differences were found in comparison with the traditional
108 mechanical (sieve) analysis **[11,16]** or the use of reflected light microscopy (RLM) for the
109 recognition of hematite grains in materials engineering **[17]**. In addition, interesting
110 applications have been reported in batch solution crystallization processes, where images
111 captured by microscopy enabled the estimation of the time-varying particle size distribution
112 of particles in suspension, through crystallization experiments **[18]**. After using image
113 processing and analysis, it was also possible to determine simultaneous occurrence of
114 particulate events such as nucleation, breakage, and aggregation, in order to monitor and
115 control the properties of crystalline products **[18]**. In this sense, the application of confocal
116 microscopy and multiple sensors for dynamic measurements of crystal properties, such as
117 size, shape, and polymorph, allows relevant attributes to be determined, related not only to
118 downstream processes (filtration, washing, granulation, drying, grinding, transportation,
119 storage, and tableting), but also to end-use properties, such as bulk density, mechanical
120 strength of a tablet, catalytic activity, stability, wettability, and flowability **[19]**.

Consequently, the application of image processing and analysis for aggregate size and shape determinations could be beneficial for the mining , comminution, and materials handling industries. In particular, the efficiency of these technologies is located in their capacity to make measurements without disrupting production streams, as traditional sieving methods do. Additionally, measurements can be made in real time, so that appropriate adjustments to the comminution and screening processes can be made in real time, before large quantities of out-of-specification materials are produced **[20]**.

Among the advantages of microscopy over other techniques, is the fact that it is less expensive than the others – in terms of capital costs -and in particular the fact that it makes the particle size and shape visible, without any intervention during the analysis. Its disadvantages, however, mainly relate to the reliability of its measurements, that is, for selecting the representative number of particles measured **[14,21,22]**. Furthermore, in some cases it is difficult to determine whether two or more particles are ‘‘touching” or if they are permanently stuck together and, therefore, must be considered to be one bigger particle **[19]**. In addition, some authors emphasize that the sampling preparation, acquisition, and nature of images, image processing, such as linear filters, rank filters, and morphological filters,play a key role **[12]**. All of the considerations mentioned are essential in the variability of the measurement. However, there are several statistical tools that one may use to address the disadvantages mentioned above and to validate that the microscopic measurement is representative. In this regard, analysis of the variability between the images per sample and between samples will allow it to be determined whether there are significant differences between the distribution of particles or aggregates size that were measured. Depending on the data distribution (normal distribution or not), parametric and non-parametric statistics can be used to compare the population group (data within images or between images).

Peer-reviewed version available at Minerals 2019, 9, 724; doi:10.3390/min9120724

The aim of this study was to apply a non-invasive method to quantify the size distribution of aggregates using optical microscopy and semiautomated image processing and analysis. This valuable information can be a useful tool for measuring, in a more realistic manner, the aggregate size distribution and the critical parameter when designing optimal operational conditions for the solid-liquid separation processes.

2. Methodology

2.1 Reagents

The reagents used in this study (NaCN, CuCN, NaHS, NaOH, and H_2SO_4) were analytical grade chemicals obtained from Merck and Sigma Aldrich. All solutions were made using demineralized water (<1 µS). The pH electrode (Methrom, Model 913) was calibrated using pH buffer solutions (Hanna).

2.2 Generation of precipitation aggregates

The precipitation aggregates generated were sulfide copper, which was produced from synthetic cyanide solutions, simulating the typical operational conditions of the SART (Sulfidization, Acidification, Recycling, and Thickening) process. This technology has been designed to recover copper and cyanide from cyanide solutions in gold mining **[5,23]**, according to the following general chemical reaction:

$$2\ Cu(CN)_3^{-2} + 3\ H_2SO_4 + S^{-2} \leftrightarrow Cu_2S_{(s)} + 6\ HCN_{(aq)} + 3\ SO_4^{-2} \quad (1)$$

The synthetic cyanide solution was made by mixing NaCN, CuCN, and NaOH to adjust the pH value at 12, avoiding HCN volatilization. The copper and total cyanide concentration were fixed at 1800 mg/L and 2460 mg/L, respectively. The copper concentration was chosen

based on the copper concentrations found in gold mining, which have high cyanide-soluble copper content in the ore **[5,24-26].** Moreover, the cyanide concentration was defined according to the cyanide associated to copper, in order to keep a free cyanide concentration of 100 mg/L; a typical value set in gold mining operations to ensure gold dissolution **[2,27]**. This value was estimated from the thermodynamic equilibrium of the copper-cyanide complexes by using the software Hydra/Medusa from the KTH Royal Institute of Sweden **[28]** The sulfidization reaction (Equation 1) was carried out in a glass reactor of 650 mL capacity over a period of 15 minutes, setting the pH at 4.0 and sulfide dosage at 120% stoichiometric, using 1 M sulfuric acid and NaHS dosage, respectively. These conditions were selected with the aim of ensuring the maximum precipitate generation according to literature **[5]**.

2.2 Size distribution analysis techniques

2.2.1 Laser diffraction analysis

A 600 mL sample of a suspension which resulted from the sulfide precipitation was analyzed by the laser diffraction technique, using a Malvern Mastersizer 2000 (MM2000). The aim was to measure the particle size distribution (PSD) of the suspended solids (i.e., copper sulfide precipitates). The Mastersizer equipment uses an agitated tank which operates at 1000 rpm. The sample is recirculated by a centrifugal pump (2500 rpm), in order to keep the solids suspended and homogenized in the suspension. Additionally, the supplier of the Mastersizer 2000 (MM2000) recommends the use of an additional pre-treatment of ultrasound at 20 KHz during 1 minute, during which suspended particles form aggregates **[29].**

2.2.2 Microscopy and semiautomated image processing and analysis

Peer-reviewed version available at Minerals 2019, 9, 724; doi:10.3390/min9120724

The particle size distribution (PSD) of aggregates was measured using an optical microscope (Leica DM 750) connected to a digital camera HD 5 MGPXL WI-FI (Leica ICC50W), which captured the images. The size distribution estimate was determined using two software for image processing. The Leica Application Suite V4 12 was used to measure the equivalent diameter of the aggregates up to 320 µm, whereas aggregates with an equivalent diameter larger than 320 µm were analyzed using the software Image Pro Plus 6. After these analyses, the complete PSD was estimated by mixing the distribution curves obtained from both software. The image-processing and analysis was carried out using two software, in order to ensure the precision of the measurements in a wide range of diameter sizes.

It is crucial that samples are representative, in order to give reliable information for process-control purposes. Taking this issue into account and adding the fact that copper sulfide precipitates tend to form aggregates rapidly, the suspension sampling and the image-capture must be carried out in a short time span. Hence, when the sulfidization reaction was completed (after 15 min), the suspension sampling and image-capture were performed in a maximum time period of two minutes. Samples were taken at the same level of the agitated reactor, using a siringe connected to a 7 mm tubing to avoid the destruction of aggregates. In this time, it was possible to capture nine images (M1 to M9 images), which were obtained from 70 µL of suspension collected from the reactor. These samples were placed on three zones of the microscope slide in order to be analyzed by the optical microscope.

2.3 Measurement of copper content in the sulfide precipitate

The copper sulfide precipitate obtained during the sulfidization reaction was characterized by a scan by an electron microscope coupled with an energy-dispersive X-ray (SEM-EDX),

Peer-reviewed version available at Minerals 2019, 9, 724; doi:10.3390/min9120724

214 JEOL model IT300 LV. With this analysis, the copper content in the precipitate generated
215 was quantified.
216
217 ***2.4 Copper sulfide conversion***
218 A sample of the suspension was taken from the sulfidization reactor during each 15-min
219 reaction interval. This sample was filtered using a syringe filter of 0.22 µm pore size. The
220 solution collected was neutralized at pH 12 with a 1M NaOH solution. The dissolved copper
221 was measured using an atomic absorption spectrometer (AAS),GBC model SensAA dual.
222 The copper concentration measured in the sample was used to estimate the conversion of
223 sulfide copper precipitate (copper recovery), considering the initial copper concentration in
224 the cyanide solution. Moreover, the total suspended solids (TSS) was estimated using the
225 following equation.

$$\text{TSS} = \frac{\text{Initial copper concentration} \times \text{Copper conversion}}{\text{Copper content}} \quad (2)$$

226 ***2.5 Statistical analysis***
227 For the PSD estimation, data obtained from images captured using optical microscopy (MC)
228 comprised nine images (M1….M9), from which 192 objects were randomly chosen (particles
229 were measured by a proper methodology according to their size, as previously described).
230 Furthermore, the PSD measurements made using the laser diffraction technique (MM2000)
231 were divided into two groups: (i) samples without pre-treatment (MS1) and (ii) samples pre-
232 treated by the use of sonication (MS2). Thus, 556 and 377 objects formed the population of
233 MS1 and MS2, respectively. Then, the first step was to analyze the data distribution (test
234 normal distribution) for the PSD obtained by optical microscopy and laser diffraction
235 technique, for the samples with and without pre-treatment. The exploratory data analysis,

which determines whether the data has a normal distribution, is crucial for adequately selecting the parametric or non-parametric statistics. This is because many statistical procedures, including correlation, regression, *t* test and the analysis of variance ANOVA (parametric tests), are based on the assumption that the data follows a normal distribution. In the case of abnormally distributed data, the use of parametric statistics does not allow accurate and reliable conclusions to be drawn **[30]**. In this regard, the normality was evaluated by two common and robust non-parametric statistics for this purpose:: modified Kolmogorov-Smirnov (K-S) and Shapiro-Wilk (S-W). After determining the data distribution, multiple comparison tests were conducted in order to determine whether there were significant differences between the data obtained by optical microscopy and those obtained by the laser diffraction technique for PSD. From a statistical point of view, these are crucial for guaranteeing that optical microscopy can be used as a valid technique for PSD analysis. In the case of images obtained by microscopy (M1…M9), the comparison was carried out by the analysis of variance ANOVA (parametric test) and Kruskal Wallis, which is the equivalent non-parametric statistic for one-way ANOVA **[31].** In cases where ANOVA and Kruskal Wallis reject the null hypothesis, this means that there are significant differences between the PSD on the microscopy images. It is then necessary to perform additional analysis (post-hoc test) to clarify the differences between particular pairs of experimental groups. Tukey´s HDS (honestly significant difference) procedure was used as a post-hoc test because it allows multiple comparisons of the mean to be performed, in order to evaluate whether there are significant differences between the means at 95% of confidence level. The same procedure was performed for the data comparison between microscopy and laser diffraction technique, with and without pre-treatment as well as for the validation test using non-aglomerated material as CuCN.

2.6 Validation of method using an unbiased sample

Considering the aggregation behavior of copper precipitates and the effect of time measurement on the PSD, a validation procedure was performed, in order to estimate the error of the method proposed in this study with respect to the MM2000, using an unbiased sample. For this purpose, a sample of an insoluble salt in water without aggregation behavior (CuCN, the same used for synthetic solutions) was used to validate the measure of PSD by microscopy. In this sense, a suspension of 1 g/L of CuCN was prepared using demineralized water. The method of data acquisition by microscopy employed was the same as the method described in section 2.2.2. The statistical procedure employed was the same as the procedure described in section 2.5.

3. Results and discussion

3.1 Generation of precipitation aggregates

The results of the reaction conversion and the copper content obtained from the sulfidization reaction are shown in Table 1. A maximum precipitate generation of 99.97% was reached for the operational conditions assessed, and it was possible to obtain a precipitate quality with 67.69 % w/w of copper content, as found in other SART studies or industrial plants **[5]**. After determining the copper content and conversion, this data was used to estimate the TSS generated in the reaction, which reached a value of 2,658 mg/L.

3.2 Size distribution analysis

From the distribution curves, the particle size was estimated at 50% distribution (P50) and 90% (P90) for all conditions studied (see Table 2). Size data were obtained by laser

284 diffraction using the MM2000 for samples with and without pre-treatment, and by image
285 processing and analysis obtained from samples studied by optical microscopy. The samples
286 pre-treated with sonication (20 kHz), as suggested by the supplier, showed the lowest particle
287 sizes prior to particle size measurement using the MM2000 (6.9 and 17.4 µm for P50 and
288 P90, respectively), in comparison with the samples analyzed by optical microscopy (119 and
289 307 µm, respectively) and the samples analyzed by laser diffraction without sonication (25.7
290 and 59.6 µm, respectively). It is important to mention that the use of sonication is indeed a
291 pre-treatment, as recommended by the supplier. This pre-treatment is carried out with the
292 aim of ensuring good particle size measurements, thereby avoiding aggregation effects in the
293 results. However, the differences observed in the values of particle sizes among the three
294 methods can be explained by the influence of external forces on the samples prior to
295 measuring the particle size, particularly in both cases of MM2000 (agitation, pumping, and
296 sonication). In fact, the sonicated samples presented smaller particle sizes due to
297 disaggregation effects promoted by the sonication, generating fine particles. This
298 methodology can be useful as an informative backup. However, it can yield impractical
299 results for equipment design and process control purposes, since the particles with
300 aggregation behavior will form new aggregates when sonication or other external forces
301 (agitation, pumping) are stopped. Therefore, the results obtained from image analysis
302 captured by optical microscopy are non-invasive. These results can thereby determine more
303 realistic particle sizes of the aggregates. Thus, the P50 size determined by microscopy is
304 around 17 times higher than the MM2000 analysis with pre-treatment, and almost 5 times
305 higher than the MM2000 results without pre-treatment. Figure 1 shows the cumulative size
306 distribution curves obtained with the three methods (MC, MS1 And MS2), where the size
307 distribution resulting from image analysis obtained by microscopy reached values higher

than 400 µm, presenting a curve with reduced slope between values 100 and 400 µm. Also, 40% of aggregates are smaller than 30 µm in size. Moreover, the disaggregation effect that occurs when using the MM2000 determines a PSD with a high quantity of fine particles.

The method of measurement for particle size by optical microscopy was also useful for observing the aggregation evolution over time, specifically when fine particles agglomerate to form new, larger aggregates. In the case of copper sulfide precipitates, the attraction forces promote rapid aggregation among particles. Therefore, the image capture must be very fast. Figure 2 shows the optical micrographs captured by the camera for M1 and M9 samples. In this case, M9 had a higher quantity of aggregates with fewer fine particles around the large aggregates. Figure 3 shows the D50 with respect to the time, from M1 to M9 (at 2 min). The particle size increases drastically from M7, indicating the increase of aggregates, although the behavior in samples M1 to M6 is parabolic, demonstrating a variable behavior. In this context, the validation of the method proposed for measuring particle size distribution is fundamental to support the representativity of the samples taken from a process.

3.3 Statistical analysis of the particle size distribution for copper aggregates

The analysis of size distribution for samples studied by optical microscopy and laser diffraction technique is shown in Table 3. It is appreciated that none of the techniques used for PSD characterization have shown a normal distribution. This is an indication of the complexity of the aggregates and the variability that can be found in the distribution. Figure 4 shows the distribution of all the images (M1…M9) in a Box-and-Whisker plot. In this figure not only is it confirmed that the distribution is not normal, but also it is shown that two of the images (M1 and M8) have 50% of the data located in the range of 160-340 µm in comparison with the rest of the images in which 50% of the data are located in a PSD lower

Peer-reviewed version available at Minerals 2019, 9, 724; doi:10.3390/min9120724

than 160 μm. This can be explained by the fact mentioned above, namely, that the precipitates obtained in the sulfidization process tend to aggregate over time.Therefore fewer small particles are quantified by the image analysis during the image capture.The aggregates grow over time, changing the size distribution.

According to the non-parametric Kruskal-Wallis, there are significant differences between the images (F-ratio=27.35; p-value=0.0006). Additionally, ANOVA analysis showed that there are significant differences (F-ratio=4.12; p-value=0.0002) between the images (M1….M9) obtained by optical microscopy. However, those differences do not appear in all the images. Figure 5 shows the Tukey´s HDS plot for the PSD by optical microscopy, in which it is observed that images M1 and M8 exhibited differences from the other images. The differences observed in these images with respect to the other images can be attributed to the aggregation behavior of precipitates over time. In this case, the M1 image was measured first and M8 was captured closer to the defined time-limit for taking the picture (2 min). Therefore, the size of the aggregates is greater than in the other samples. (The 2 min time could be variable for different particles. This will depend on the aggregation characteristics.)

Considering that M1 and M8 showed a different distribution, these images were removed from the analysis, since the time that elapsed affected the representativity of these samples, maximizing the size of aggregates with respect to the real-time expended in the reactor. ANOVA and Kruskal-Wallis results without M1 and M8 showed that there are no significant differences between the images for the ANOVA (F-ratio=1.87; p-value=0.0903) and the Kruskal-Wallis test (F-ratio=1.7266; p-value=0.1163). This means that the distribution obtained is representative from a statistical point of view. Additionally, Levene's statistic was calculated in order to determine whether there are significant differences between the

356 standard deviation of the seven images. Results obtained for this statistic showed that there
357 are no significant differences (F-ratio=1.7266; p-value=0.1188) within the standard deviation.
358 Thus, the standard deviation obtained from the seven images is representative at 95% of
359 confidence level.
360 The validated PSD obtained by optical microscopy was compared with the analysis of the
361 laser diffraction technique with and without pre-treatment. ANOVA and Kruskal-wallis
362 analysis showed significant differences between the PSD ($p \leq 0.05$). Figure 6 shows the
363 Tukey´s HDS plot in which significant differences between optical microscopy and laser
364 diffraction technique with and without pre-treatment can be observed. It is particularly
365 interesting that the pre-treatment applied to the sample has a significant impact on the PSD.
366 The sample in which a previous sonication (MS2) was applied showed the lower mean of
367 16.2449 µm with a standard deviation of 3.699 µm, whereas the sample without sonication
368 has a mean of 60.226 µm and a standard deviation of 3.046 µm. Considering that PSD plays
369 a crucial role in the solid-liquid separation processes, the type of analysis must be carefully
370 considered, because the pre-treatment and the type of analysis themselves generate variability
371 in the PSD characterization.
372 Furthermore, images obtained by optical microscopy (seven images) showed higher values
373 in the mean (119.721 µm) in comparison with the laser diffraction technique. This result can
374 be explained by the fact that the optical microscopy is not an invasive measurement technique.
375 Therefore, the PSD obtained by optical microscopy represents reality effectively.This is
376 crucial in the selection and design of solid-liquid separation processes. Finally, Figure 7
377 shows the definitive PSD obtained for the six first images (P50=70 µm; P90=190 µm),
378 comparing it with the MM2000 PSD results. The curve obtained with optical microscopy
379 presents two main zones of particles or aggregates, one representing the fine particles (<70

µm) and another one representing the larger aggregates (>70 µm). The limit of these two zones and their values of P50 should be the relevant information for use in solid-liquid separation process of precipitates.

3.4 Validation of method using an unbiased sample

Results of the comparative analysis for the CuCN sample are shown in Figure 8, where a Tukey´s HDS plot for the nine images obtained for CuCN sample is compared with laser diffraction technique measurement (MS). In that Figure, it is observed that there are no significant differences (p=0.11699 in ANOVA) between the images (M1…M9) and between them and the laser diffraction technique measurement (MS), as well. This means that microscopy is a validated statistical technique as a non-invasive method for the PSD determination.

4. Conclusions

Image processing and analysis using optical microscopy, coupled with statistical methods to validate the results, is a non-invasive and reliable alternative to conventional methods for quantifying the PSD of slurries containing solids with aggregation behavior, generated from precipitation processes. Furthermore, the method presented in this study is easy to implement for research and industrial purposes in a standard laboratory. Additionally, this methodology could also be used to determine PSD for different fine particles (ranging between 1 and 500 µm), as an alternative to conventional methods. Therefore, this methodology could be the basis for the application of image processing and analysis to measure PSD in different processes online, in order to improve the control and performance of solid-liquid separation equipment.

Acknowledgments

The authors gratefully acknowledge the financial support of the National Commission for Scientific and Technological Research (CONICYT Chile) through the CONICYT-PIA Project AFB180004 and the FONDEF/IDeA Program, FONDEF/CONICYT 2017+ID17I10021.

References

1. Habashi, F. Handbook of Extractive Metallurgy Vol. 1-4, 1997. Wiley-VCH, Weinheim, Germany.
2. Walton, R. Zinc cementation. In Gold Ore Process, 2nd ed.; Adams, M.D., Ed.; Elsevier. 2016. Amsterdam, The Netherlands, 553–560. https://doi.org/10.1016/B978-0-444-63658-4.00031-1
3. Akcil, A., Koldas, S. Acid Mine Drainage (AMD): causes, treatment and case studies. J Clean Prod 2006, 14, 1139-1145. https://doi.org/10.1016/j.jclepro.2004.09.006
4. Fu, F., Wang, Q. Removal of heavy metal ions from wastewaters: A review. J Environ Manage 2011, 92, 3, 407-418. https://doi.org/10.1016/j.jenvman.2010.11.011
5. Estay, H. Designing the SART process – A Review. Hydrometallurgy 2018, 176, 147-165. https://doi.org/10.1016/j.hydromet.2018.01.011
6. Mokone, T.P., van Hille, R.P., Lewis, A.E. Effect of solution chemistry on particle characteristics during metal sulfide precipitation. J Colloid Interface Sci 2010, 351, 10-18. https://doi.org/10.1016/j.jcis.2010.06.027
7. Mokone, T.P., Lewis, A.E., van Hille, R.P. Effect of post-precipitate conditions on surface properties of colloidal metal sulphide precipitates. Hydrometallurgy 2012, 119-120, 55-66. https://doi.org/10.1016/j.hydromet.2012.02.015
8. Martin, A., Fawcett, S., Kulczycki, E., Loomer, D., Al, T., Rollo, A. Application of High-Resolution Microscopy Methods to the Analysis of Fine-Grained and Amorphous Treatment Sludges. Proceedings Tailings and Mine Waste, 2011, Vancouver, BC, Canada, 6-9 November.

9. Fleming, C.A., Melashvili, M. The SART process: killing the sacred cows. In: XXVIII International Mineral Processing Congress (IMPC 2016), Quebec, 2016, Canada, 11-15 September.

10. Greet, C.J., Smart, R. st.C. The effect of separation by cyclosizing and sedimentation/decantation on mineral surfaces. Miner Eng 1997, 10, 995-1011. https://doi.org/10.1016/S0892-6875(97)00079-4

11. Arasan, S., Akbulut, S., Hasiloglu, A.S. Effect of particle size and shape on the grain-size distribution usingImage analysis. Int J Civ Struct Eng 2011, 1, 968-985. doi:10.6088/ijcser.00202010083

12. Coster, M., Chermant, J.L. Image analysis and mathematical morphology for civil engineering materials. Cem. Concr. Compos. 2001, 23, 133–151. https://doi.org/10.1016/S0958-9465(00)00058-5

13. Ghasemy, A., Rahimi, E., Malekzadeh, A. Introduction of a new method for determining the particle-size distribution of fine-grained soils. Meas. J. Int. Meas. Confed. 2019, 132, 79–86. https://doi.org/10.1016/j.measurement.2018.09.041

14. Ramírez, C., Troncoso, E., Muñoz, J., Aguilera, J.M. Microstructure analysis on pre-treated apple slices and its effect on water release during air drying. J. Food Eng. 2011, 106, 253–261. https://doi.org/10.1016/j.jfoodeng.2011.05.020

15. Orrego, M., Troncoso, E., Zúñiga, R.N. Aerated whey protein gels as new food matrices: Effect of thermal treatment over microstructure and textural properties. J. Food Eng. 2015, 163, 37–44. https://doi.org/10.1016/j.jfoodeng.2015.04.027

16. Graham, D., Rice, S.P., Reid, I. A transferable method for the automated grain sizing of rivergravels. Water Resour Res 2005, 41, W07020, 1-12. doi:10.1029/2004WR003868

17. Alvarez-Iglesias, J.C., Gomes, O., Paciornik, S. Automatic recognition of hematite grains under polarized reflected light microscopythrough image analysis. Min Eng 2011, 24, 1264-1270. https://doi.org/10.1016/j.mineng.2011.04.015

18. Presles, B., Debayle, J., Févotte, G., Pinoli, J.C. Novel image analysis method for in situ monitoring theparticle size distribution of batch crystallization processes. J Electron Imaging 2010, 19(3), 031207. DOI: 10.1117/1.3462800

19. Singh, M.R., Chakraborty, J., Nere, N., Tung, H.H., Bordawekar, S., Ramkrishna, D.

Image-Analysis-Based Method for 3D Crystal Morphology Measurement and Polymorph Identification Using ConfocalMicroscopy. Crist Growth Des 2012, 12, 3735-3748. DOI: 10.1021/cg300547w

20. Maerz, N.H. Aggregate sizing and shape determination using digital image processing. CenterFor Aggregates Research (ICAR)Sixth Annual Symposium Proceedings, 1998, St. Louis, Missouri, April 19-20, 195-203.

21. Ramírez, C., Young, A., James, B., Aguilera, J.M. Determination of a representative volume element based on the variability of mechanical properties with sample size in bread. J. Food Sci. 2010, 75, 516–521. https://doi.org/10.1111/j.1750-3841.2010.01805.x

22. Ramírez, C., Aguilera, J.M. Determination of a representative area element (RAE) based on nonparametric statistics in bread. J. Food Eng. 2011, 102, 197–201. https://doi.org/10.1016/j.jfoodeng.2010.08.021

23. MacPhail, P.K., Fleming, C., Sarbutt, K. Cyanide Recovery by the SART Process for the Lobo-Marte Project, Chile. Randol Gold and Silver Forum, 1998, Denver (April 26-29).

24. Botz, M., Acar, S.Copper Precipitation and Cyanide Recovery Pilot Testing for the Newmont Yanacocha Project. In: Society for Mining, Metallurgy & Exploration (SME) Annual Meeting, Denver, 2007, February, 25–28.

25. Botz, M., Kaczmarek, A., Orser, S. Managing copper in leach solution at the Copler gold mine: laboratory testing and process design. Miner Metall Proc 2011, 28, 133-138. DOI: 10.1007/BF03402245.

26. Estay, H., Carvajal, P., Hedjazi, F., Van Zeller, T. The SART process experience in the Gedabek plant. In: HydroProcess, 4th International Workshop on Process Hydrometallurgy, 2012, Santiago, Chile.

27. Marsden, J.O., House, C.I. The Chemistry of Gold Extraction. Second ed., Society for Mining, Metallurgy and Exploration SME, 2006, Colorado, USA.

28. Puigdomenech, I. Hydra-Medusa Software (Hydrochemical Equilibrium Constant, Database and Make Equilibrium Diagrams Using Sophisticated Algorithms), version 1; Inorganic Chemistry, 2004. Royal Institute of Technology: Stockholm, Sweden.

29. Malvern Instruments Ltd. Mastersizer 2000 User Manual UK. 2007.

https://www.labmakelaar.com/fjc_documents/mastersizer-2000-2000e-manual-eng1.pdf.(Accessed 23 November 2018).

30. Ghasemi, A., Zahediasl, S. Normality tests for statistical analysis: A guide for Non-statiticians. Int J Endocrinol Metab 2012, 10(2), 486-489. doi: 10.5812/ijem.3505

31. Montgomery, D.C. Design and analysis of experiments-second edition. 2001, Qual. Reliab. Eng. Int. https://doi.org/10.1002/qre.4680030319

Figure Captions

Figure 1. Cumulative particle size distribution curve for different methods of particle size measurement. In the case of MC, it considers 9 original samples.

Figure 2. Optical micrographs of samples analyzed at different times, M1 at 10 seconds (left), M9 at 2 minutes (right).

Figure 3. Results of D50 particle size of copper precipitates with respect to the capture time of image in the microscope.

Figure 4. Box-and-Whisker plot for the PSD of nine images obtained by optical microscopy.

Figure 5. Tukey´s HDS plot for PSD by optical microscopy.

Figure 6. Tukey´s HDS plot for comparison of PSD between optical microscopy and laser diffraction technique with and without pre-treatment.

Figure 7. Cumulative particle size distribution curves for three methods of particle size measurement. In this case, the PSD obtained from image analysis by optical microscopy includes only M1 to M6.

Figure 8. Tukey´s HDS plot for comparison of PSD between optical microscopy (M1…M9) and laser diffraction technique (MS) for the CuCN sample.

528 **List of tables**

529

530 **Table 1.** Sulfidization results.

531

532 **Table 2.** Particle size estimated by optical microscopy and laser diffraction technique.

533

534 **Table 3.** Analysis of normal distribution for samples analyzed by optical microscopy and
535 laser diffraction technique.

536

Peer-reviewed version available at Minerals 2019, 9, 724; doi:10.3390/min9120724

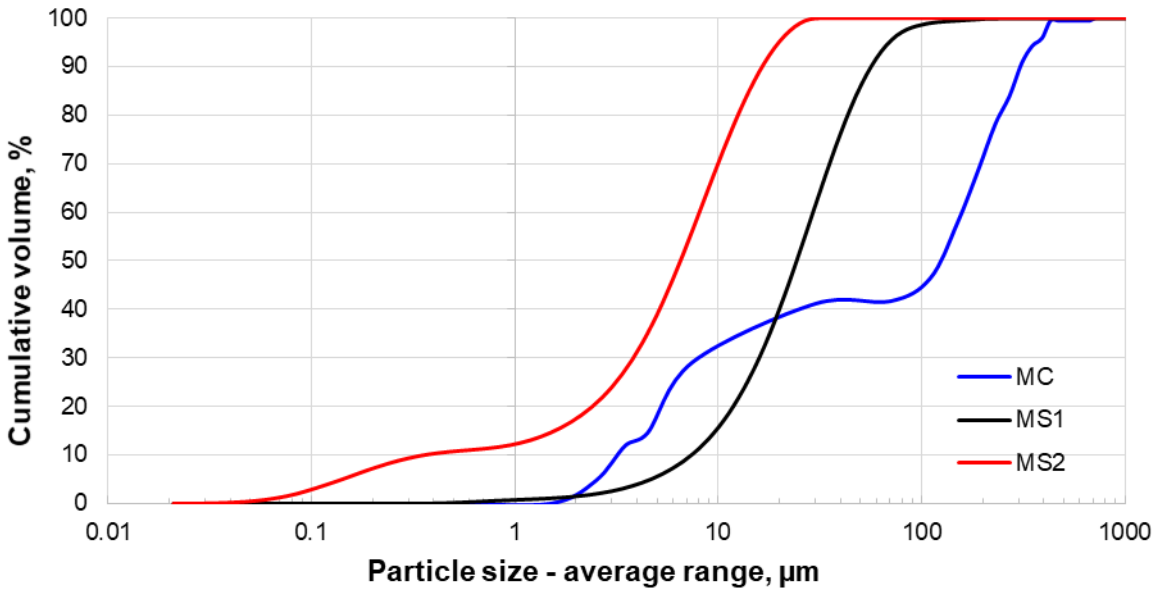

Figure 1. Cumulative particle size distribution curve for different methods of particle size measurement. In the case of MC, it considers 9 original samples.

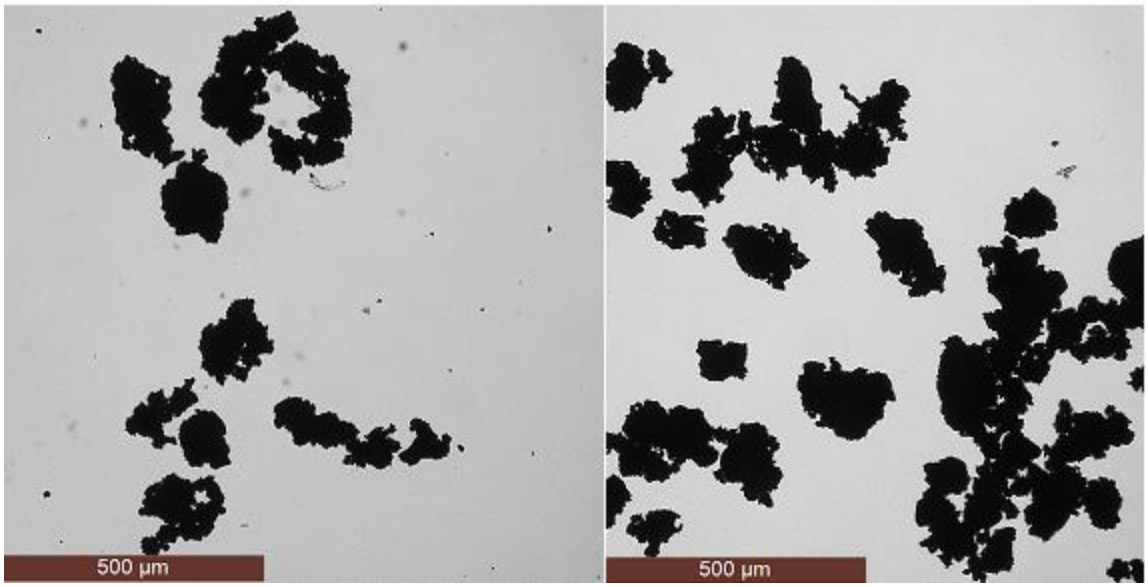

Figure 2. Optical micrographs of samples analyzed at different times, M1 at 10 seconds (left), M9 at 2 minutes (right).

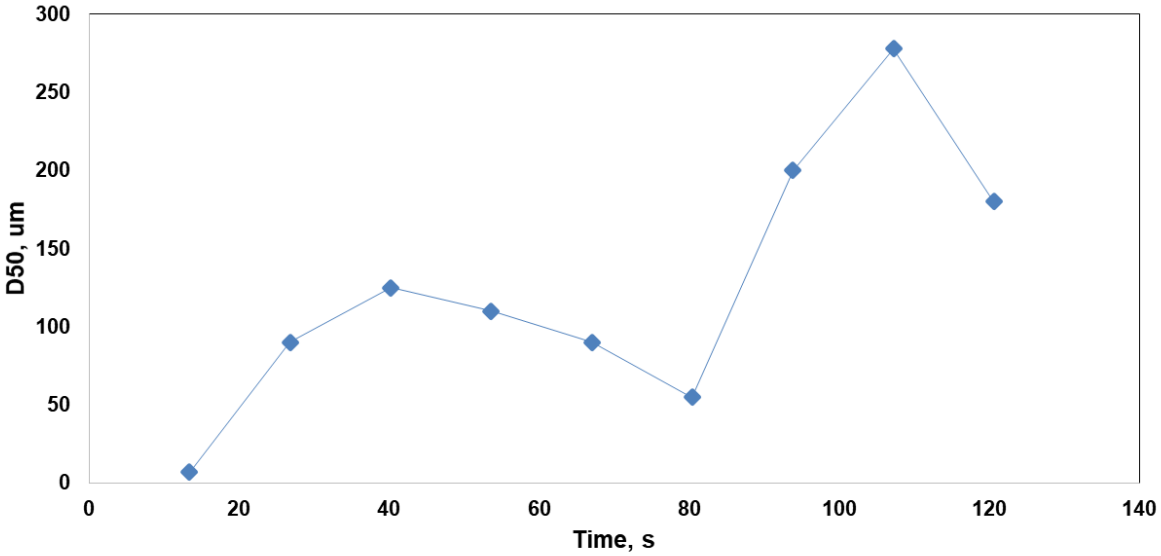

547
548 **Figure 3.** Results of D50 particle size of copper precipitates with respect to the capture time
549 of image in the microscope.

550
551

552

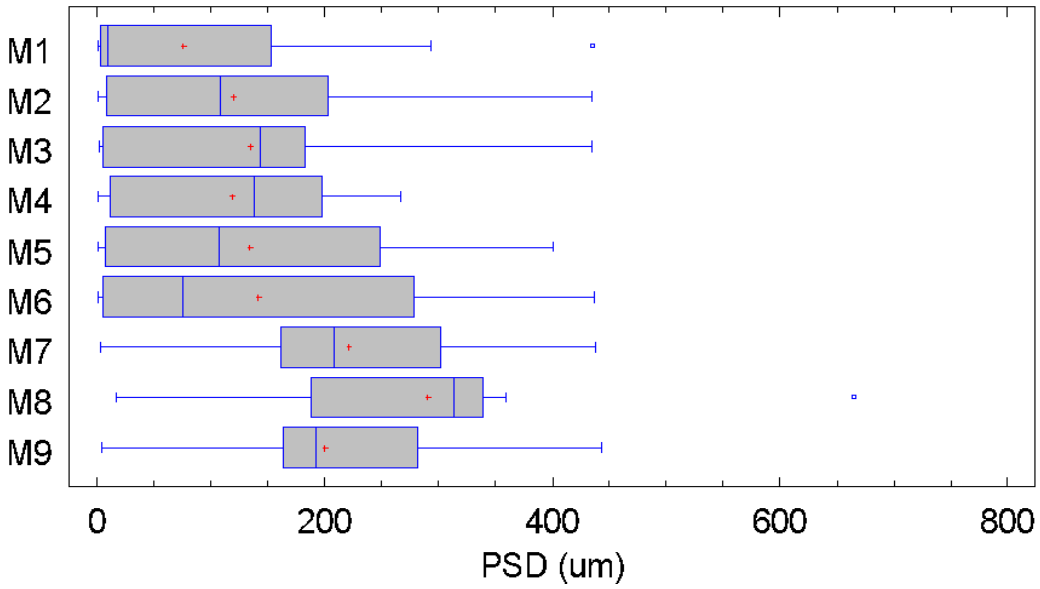

553

554 **Figure 4.** Box-and-Whisker plot for the PSD of nine images obtained by optical microscopy.

555

556

Peer-reviewed version available at Minerals 2019, 9, 724; doi:10.3390/min9120724

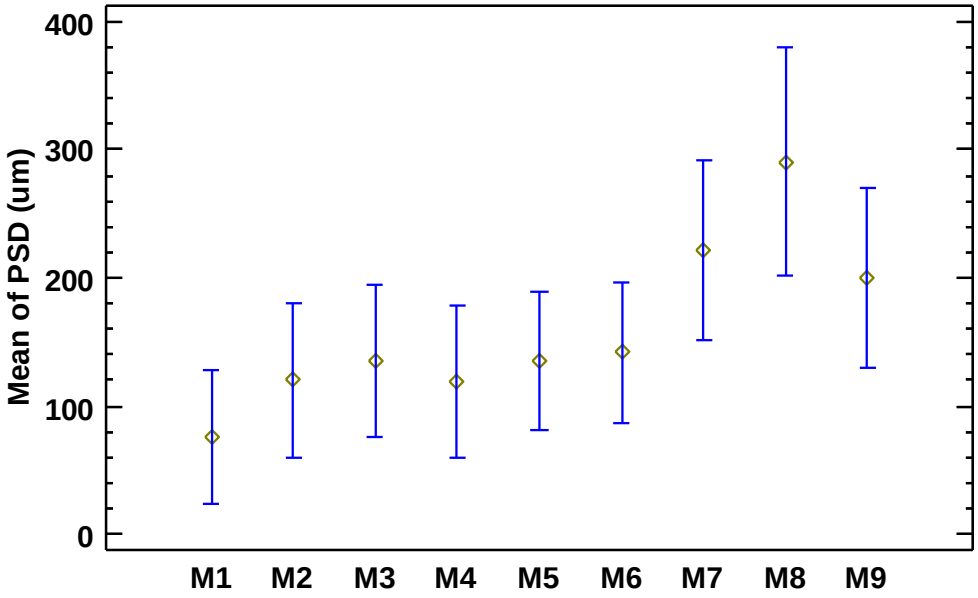

Figure 5. Tukey´s HDS plot for PSD by optical microscopy.

Peer-reviewed version available at Minerals 2019, 9, 724; doi:10.3390/min9120724

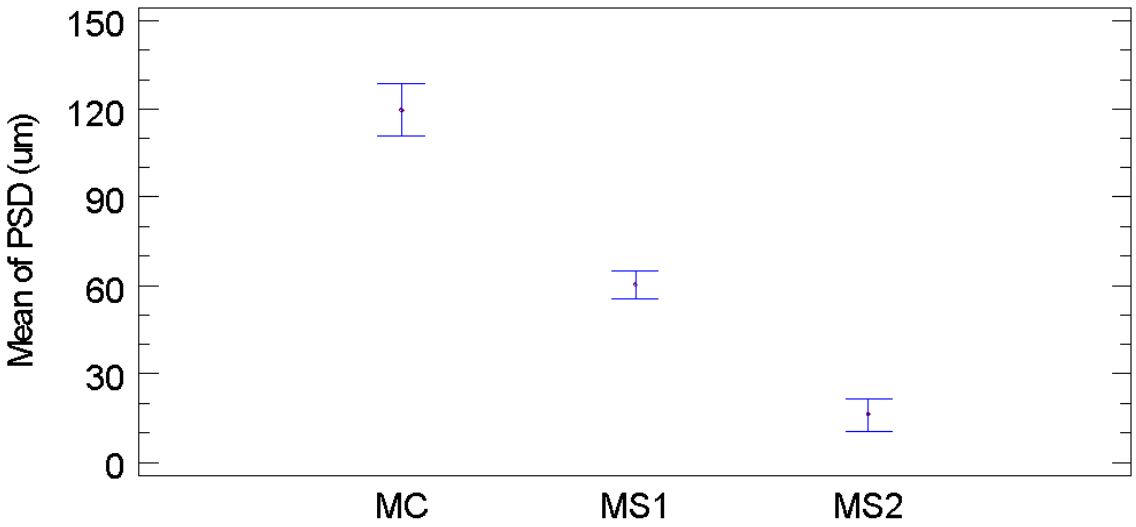

Figure 6. Tukey´s HDS plot for comparison of PSD between optical microscopy and laser diffraction technique with and without pre-treatment.

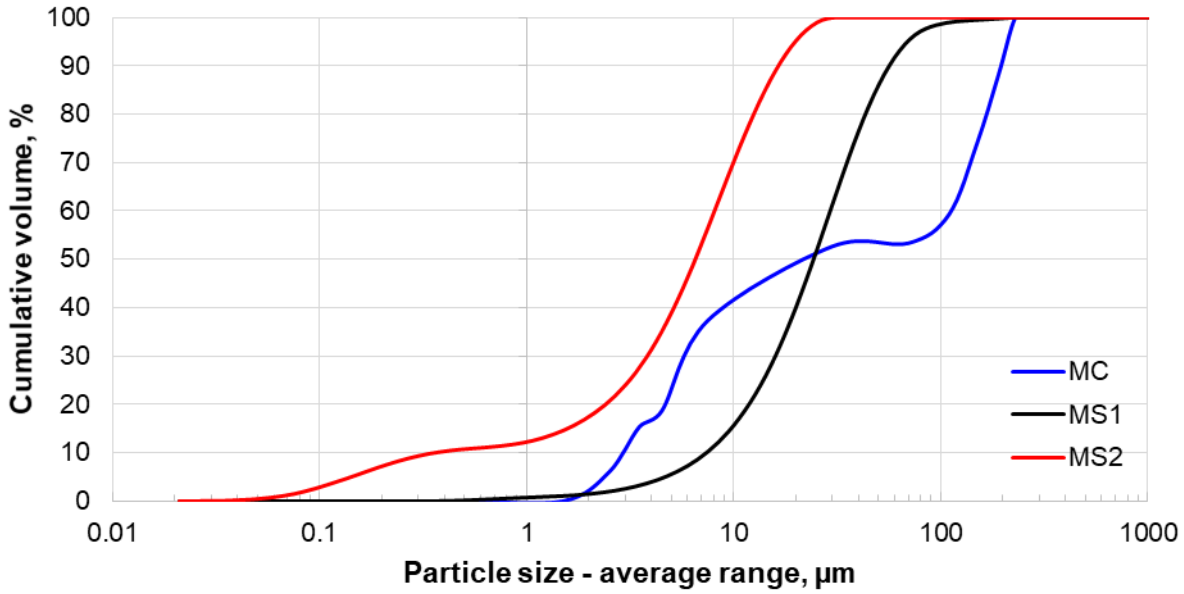

565

566 **Figure 7.** Cumulative particle size distribution curves for three methods of particle size
567 measurement. In this case, the PSD obtained from image analysis by optical microscopy
568 includes only M1 to M6.

569

Peer-reviewed version available at Minerals 2019, 9, 724; doi:10.3390/min9120724

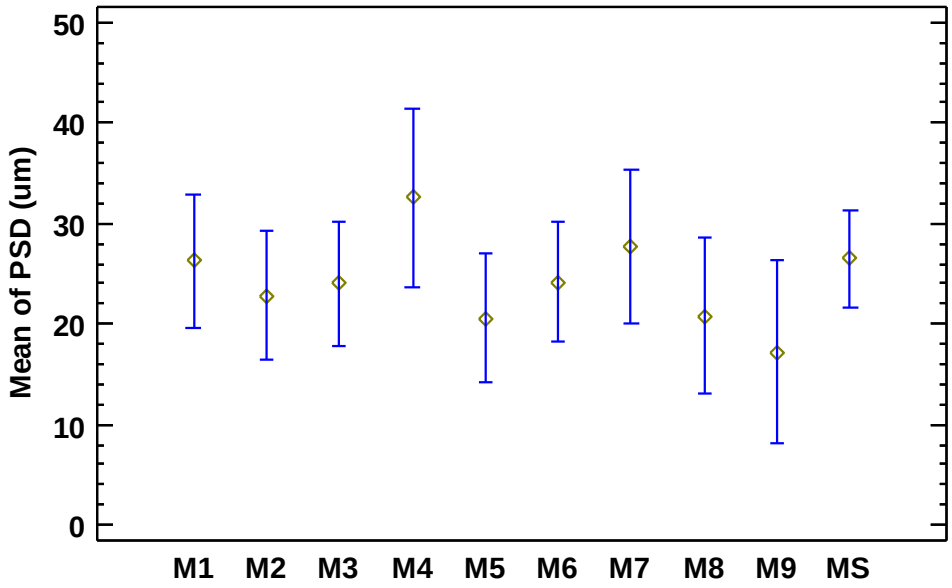

570

571 **Figure 8.** Tukey´s HDS plot for comparison of PSD between optical microscopy (M1…M9)
572 and laser diffraction technique (MS) for the CuCN sample.

573

574 **Table 1.** Sulfidization results.

575

Description	Value
Copper content, % w/w	67.69
Copper sulfide conversion, %	99.97
Total suspended solids, mg/L	2,658

576

577 **Table 2.** Particle size estimated by optical microscopy and laser diffraction technique.

Particle size, µm	MC	MS1	MS2
P50	119	25.7	6.9
P90	307	59.6	17.4

P50: Particle size at 50% distribution; P90: Particle size at 90% distribution. MC: Optical microscopy; MS1: Laser diffraction without pre-treatment; MS2: Laser diffraction with pre-treatment.

578

579

580 **Table 3.** Analysis of normal distribution for samples analyzed by optical microscopy and
581 laser diffraction technique.

Statistics	MC		MS1		MS2	
	F-ratio	p-value	F-ratio	p-value	F-ratio	p-value
Shapiro-Wilk	0.87288	<0.05	0.60841	<0.05	0.77999	<0.05
Modified Kolmogorov-Smirnov	2.73516	<0.05	5.82743	<0.05	5.03322	<0.05

MC: Optical microscopy; MS1: Laser diffraction without pre-treatment.; MS2: Laser diffraction with pre-treatment.

582